Preprint Title	Facile Synthesis of Bulk Cylinder Consolidated with Ultralong Silver Vanadate Nanowires and its Enhanced Antibacterial Activities Against Gram Positive and Gram-Negative Bacteria
Authors	Willy Klöckner, Cristian P. Vidal, Carol L. de Dicastillo, Ram M. Yadav and D. I. N. E. S. H. P. SINGH
Publication Date	02 Sep 2019
Article Type	Full Research Paper
Supporting Information File 1	Untitled.mov; 50.5 MB
ORCID® iDs	Carol L. de Dicastillo - https://orcid.org/0000-0003-0067-9765; D. I. N. E. S. H. P. SINGH - https://orcid.org/0000-0002-2893-7749

Facile Synthesis of Bulk Cylinder Consolidated with Ultralong Silver Vanadate Nanowires and its Enhanced Antibacterial Activities Against Gram Positive and Gram-Negative Bacteria

Willy Klöckner[1], Cristian Patiño Vidal[2], Carol López de Dicastillo[2], Ram Manohar Yadav[3] and Dinesh Pratap Singh[1,4]*

[1]Departament of Physics, University of Santiago Chile, Avenida Ecuador 3493, Estación Central, 9170124 Santiago, Chile

[2] Food Packaging Laboratory (Laben-Chile), Department of Science and Food Technology, Faculty of Technology, University of Santiago Chile, Obispo Umaña 050, 9170201 Santiago, Chile

[3] Department of Physics, VSSD College Kanpur, 208002, India

[4] Millennium Institute for Research in Optics (MIRO), Av. Esteban Iturra S/N, Concepción, 4030000 Concepción, Chile

***Corresponding Author:** Dinesh Pratap Singh

- **Email:** singh.dinesh@usach.cl dineshpsingh@gmail.com
- **ORCID:** 0000-0002-2893-7749

Abstract

Self-assembled 3D structures with 0, 1 or 2D nano building blocks are fascinating due to its astounding new and enhanced properties for various applications. Here we report the acetonitrile mediated synthesis of self-assembled bulk cylinder of length ~ 9.00 cm and diameter ~ 4.0 cm consolidated with ultralong and very thin silver vanadate nanowires and its enhanced antibacterial activity. The addition of acetonitrile during synthesis and its volumetric concentration plays an important role in the self-assembly. The use of 30 mL acetonitrile during the mixing of the reactants $AgNO_3$ and NH_4VO_3 and post hydrothermal treatment at 200 °C for 12 h result the formation of bulk cylinder like structure. X-ray diffraction (XRD) and Scanning electron microscopy (SEM) revealed that the bulk cylinder is consolidated with ultrathin and long β-$AgVO_3$ nanowires having minimum diameter ~16 nm and of undefined length (approximately 10 μm long). The self-assembled β-$AgVO_3$ nanowire like structure with very high surface area exhibited very high antibacterial activity against *Listeria innocua* ATCC 33090 and *Staphylococcus aureus* ATCC 25923 and *Escherichia coli* ATCC 25922, as Gram-positive and Gram-negative bacteria, respectively.

Keywords

Silver vanadate; Nanowires; β-$AgVO_3$; Self –assembly; Antibacterial; Escherichia coli

Introduction

Various silver vanadium oxide (SVO) phases depending on the oxidation states and stoichiometric /nonstoichiometric compositions of silver, vanadium and oxygen exhibit variety of crystal structures and hence strikingly new properties[1-8]. Among all silver vanadate compounds, β-$AgVO_3$ is one of the most stable structures and explored for its astounding applications in the area of sensors [9], biosensors [10], photocatalysis [11, 12], tribology [13-16], lithium ion battery [17], antibacterial applications [18, 19] and many more yet to be explored. Interestingly, the various properties of $AgVO_3$ are highly dependent to the synthesis strategies, hierarchical morphology, crystal structures, mixed phases, and surface properties of the product [20]. Lithium/silver vanadium oxide is potentially used as an efficient battery for implantable cardioverter-defibrillators which not only monitor the electrical signals from heart beat but also senses when the heart beats are irregular or dangerous [21]. Various approaches have been developed for the growth of $AgVO_3$[22, 23], modified structures and its composites to improve the desired properties of photocatalytic activities [24-28], degradation of organic pollutants [29, 30], lubricious behavior [13, 14, 16], electrochemical performance [31-34], rechargeable lithium batteries, [35] tribological behavior [36, 37], creation of SERS hot spots [36, 38, 39], organic sensors [40], tunable electric properties [41] etc. Recent advances in the synthesis of nanomaterials have created a widespread scope and strikingly new opportunities to explore its applications in the area of bio medicine and clinical research [42]. Metallic nanoparticles [43, 44], specially silver [45, 46], and gold [47, 48] have been extensively studied from their antibacterial point of view. The surface modification, functionalization or capping with various agents have shown a significant improvement on the antimicrobial efficacy. [49-54] Silver based nanostructures can be promising candidates for the development and significant improvements of new and effective antimicrobial systems due to higher adsorption at bacterial surfaces, oxidative dissolution of nanomaterials, etc. Recently, it has been found that vanadium related compounds having oxidation states of V(III), V(IV) and V(V) are of great biological relevance because of its ability to mimic phosphate groups and vice versa[55]. Highly crystalline metastable

polymorphs of $AgVO_3$ were already developed via protein inducing process by utilizing various proteins like bovine hemoglobin, bovine serum albumin, and lysozyme[56]. other works have already shown the addition of different concentrations of β-$AgVO_3$ with dental acrylic resins improved the antibiofilm activity against *C. albicans* and *S. mutans* [57]. Incorporation of TiO_2 into the $AgVO_3$ improved the photocatalytic and antibacterial activities [19]. Recently, it was reported that metastable α-$AgVO_3$ which is thermally transformed into β-$AgVO_3$ at 200 °C [5] exhibited high antibacterial activity against methicillin-*resistant Staphylococcus aureus* [58].

Self assembled silver and vanadium based compound with very high surface area can have enhanced antibacterial activity. Antimicrobial activities of self assembled structures made up with ultralong and very thin nanowires were analyzed against *Listeria innocua, Staphylococcus aureus* and *Escherichia coli* following international normative ASTM E2149-10.

Results and discussion

Structural/Microstructural Characterizations

Figure 1 shows the various optical images of the synthesized ultralong SVO nanorods consolidated into bulk cylinder as obtained after mixing the reactants followed by hydrothermal treatment. Figure 1a is the image of the resultant solution before putting in the furnace obtained after 2hrs of mixing the reactants until the pH got saturated. The solution was a homogeneous light-yellow color suspension and a part of it was also preserved separately to see any change in the structures without the hydrothermal treatment. Figure 1b is the image of the as-synthesized material just after taken out from the furnace after hydrothermal treatment. As can be seen, the structure grown, are in the form of a cylindrical shape where the bottom and surfaces are supported by the walls of the autoclave. The structure was easily transferred into a vessel filled with distilled water. Figure 1c shows the bottom view of the bulk cylinder which clearly shows the highly porous structure. The diameter of the cylinder is ~ 4.00 cm. The Top view of the open-ended cylinder can be seen in the Figure 1d. A complete view of the as obtained bulk

cylinder is shown in Figure 1e having a vertical length of ~ 9.00 cm and diameter ~ 4.00 cm.

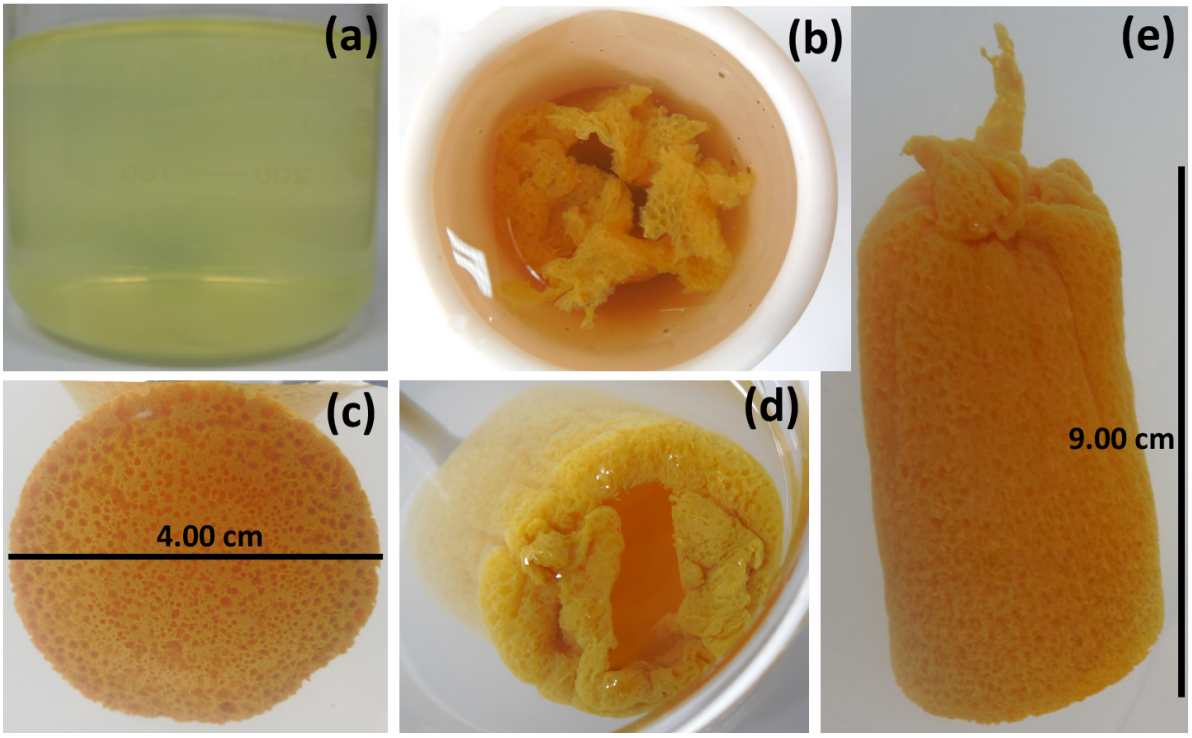

Figure 1: **(a)** As obtained suspension after mixing the reactants and pre hydrothermal treatment; **(b)** As obtained structure after hydrothermal treatment; **(c, d)** Bottom and top view of the SVO bulk cylinder having diameter 4.00 cm; and **(e)** A complete view of the as obtained SVO bulk cylinder suspending in the distilled water and having length ~ 9.00 cm.

The preserved solution before hydrothermal treatment formed hydrogel like structure which was further characterized by SEM. Figure 2 shows SEM images of the hydrogel as obtained at ambient condition without any hydrothermal treatment. Figure 2a and b show the large amount of very thin film wavy like structures. The structures resemble to the various 2D like layered structures, such as graphene and MoS_2 and WS_2, etc. The thin films were very flexible and formed into a curved shape. The magnified image 2c and 2d show that these thin films were consolidated with millions of ultrathin flexible nanorods

like structures. It seems that first the nucleation starts at room temperature and then they started to grow in the ultralong nanorods shape with flexible wavy shaped and finally self-assembled into the form of thin films like cotton threads. Although crystallinity of the nanorods is very poor and lengths are undefined due to threaded with one another.

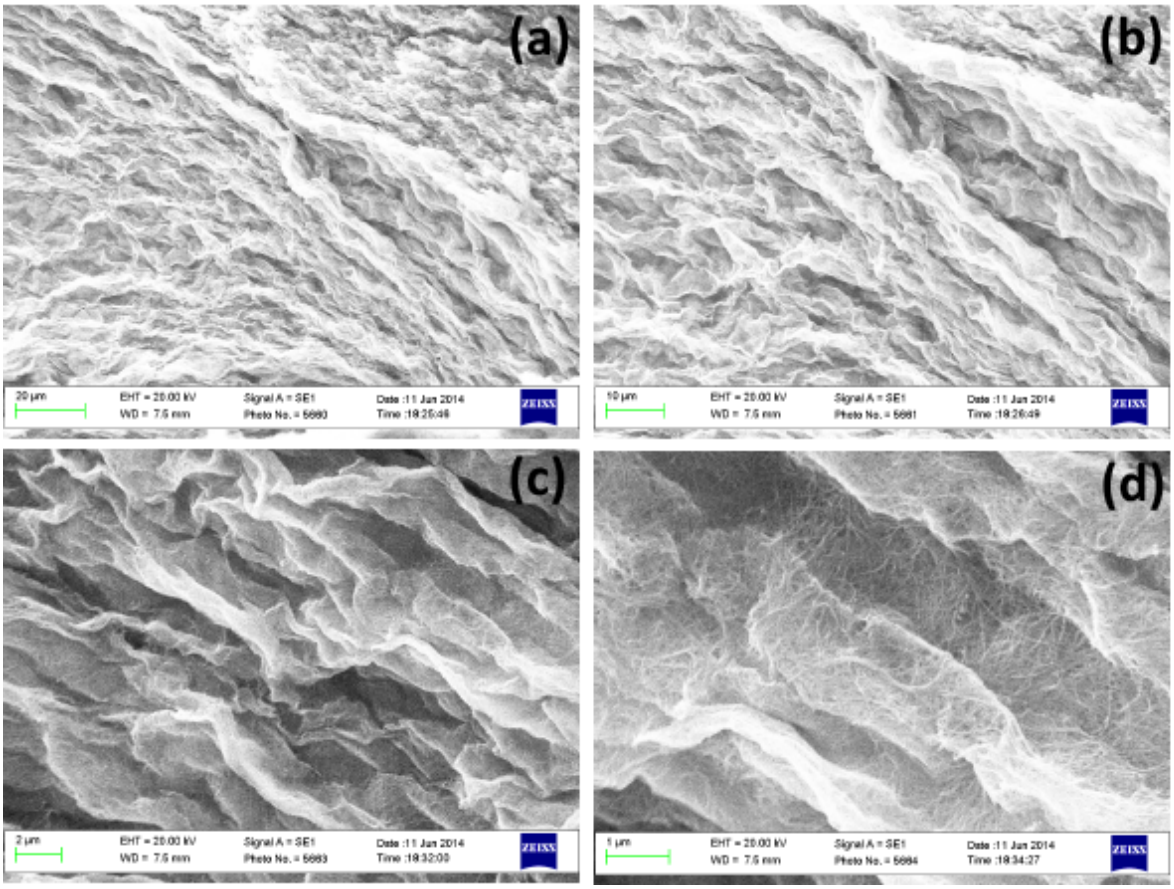

Figure 2: (a, b) Low magnification SEM images of the hydrogel as obtained without hydrothermal treatment. **(c, d)** High magnified SEM images reveal the formation of flexible undefined ultralong nanorods, self-assembled into wavy thin film like structures.

Panel of Figure 3 shows the SEM images of the as-synthesized bulk cylinder walls after samples were freeze dried. In contrast to the samples without hydrothermally treatment, a large number of nanorods with better defined shape and morphologies can be observed. The higher crystallinity was achieved by the operating hydrothermal

temperature for long time. Figure 3a and 3b show the low and high magnification images that revealed the formation of large number of nanorods like structures. Higher magnified image, as shown in Figure 3c, indicates the formation of ultralong nanowires with defined morphologies due to better crystallinity. As Figure 3d shows, the cylinders wall is interwoven by flexible nanowires having widths in the range of 16-50 nm.

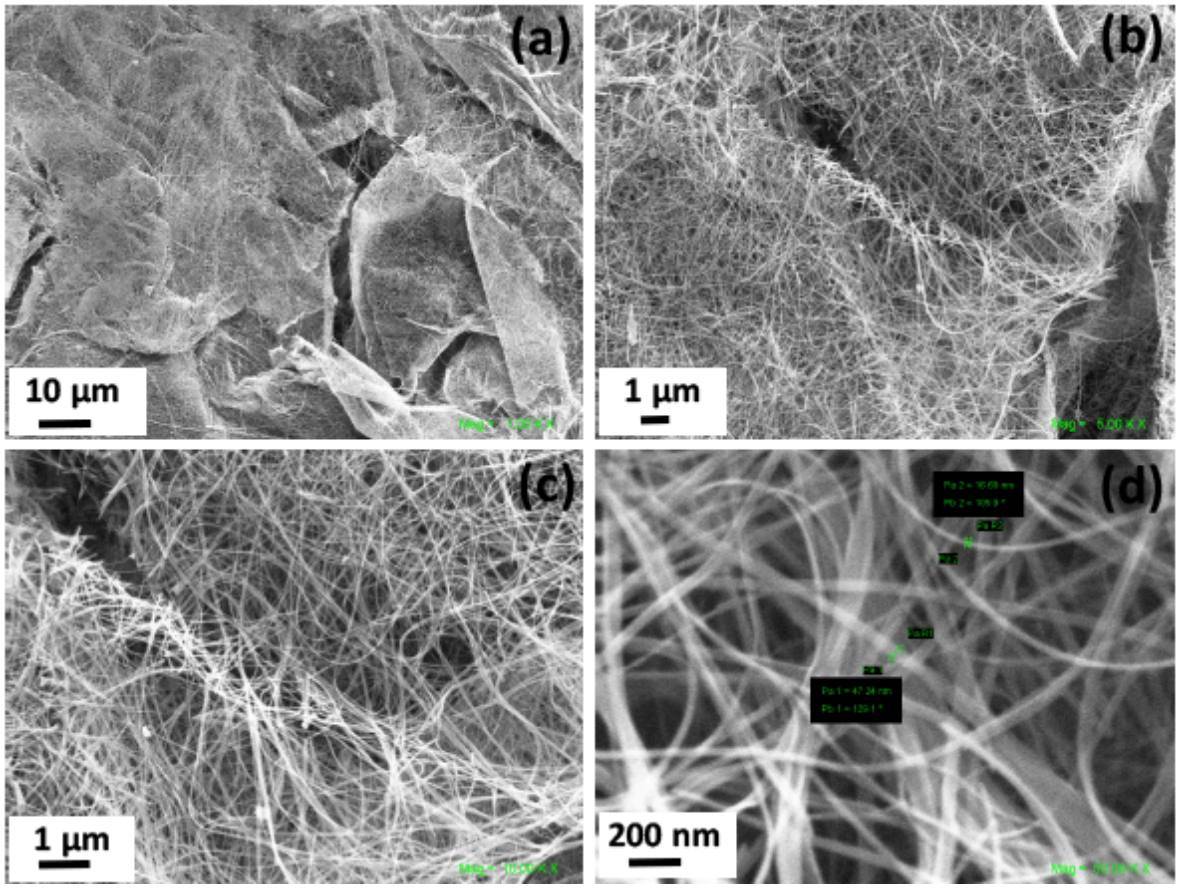

Figure 3. (a, b) Low magnification SEM image of the freeze-dried sample of the as obtained material after hydrothermal treatment; **(c, d)** High magnified images show the ultralong and flexible nanowire like structure.

The panel of Figure 4 represents the pH and Temperature variation during reaction time and also structural/spectroscopic characterizations of the as synthesized materials. The Figure 4a is the graph of pH and temperature variation versus time during the mixing of

the reactants. During the initial 5 min, the pH of the NH_4VO_3 solution suddenly dropped due to the mixing of the acetonitrile admixed $AgNO_3$ solution which gradually increased with respect to the time until gets saturated after one hour. The saturated pH was recorded ~ 6.4. A gradual increment in the temperature from 18.5 to 22 °C shows that the reaction was exothermic. After the pH saturation, the solution turned into light yellow color, as it can be seen in the Figure 1a. In absence of acetonitrile, the reaction kinetics was very fast and the yellow precipitate contained a large number of comparatively thicker and shorter α-$AgVO_3$ nanorods, as already reported by our group [15]. The presence of acetonitrile and its concentration is a critical factor for the growth of ultralong nanowires and specific form of bulk cylinder. Acetonitrile slowed down the reaction kinetics and favored the formation of large number of very small nuclei and hence the growth of ultrathin nanowires. The low concentration of acetonitrile ~ 5mL resulted into 3D spongy like circular structures reported previously by us [59]. It was noticed that without acetonitrile the reaction was quick and initially presented an orange color particle formation which turned into yellow color precipitate finally within 30 mints after mixing the reactants. Whereas in 5 mL acetonitrile, the orange color suspension was observed which got precipitated and settled down after 90 min. The 30 mL Acetonitrile solution slowed down the reaction kinetics up to a great extent and did not allow the precipitation, even after 2 h of reaction and a very light-yellow color suspension was observed before hydrothermal treatment (Figure 1a). The XRD pattern of the as synthesized material confirmed the formation of monoclinic β-$AgVO_3$ structure and all the diffraction peaks match well with JCPDS card no. 29-1154, with I2/m(12) space group (Figure 1b).

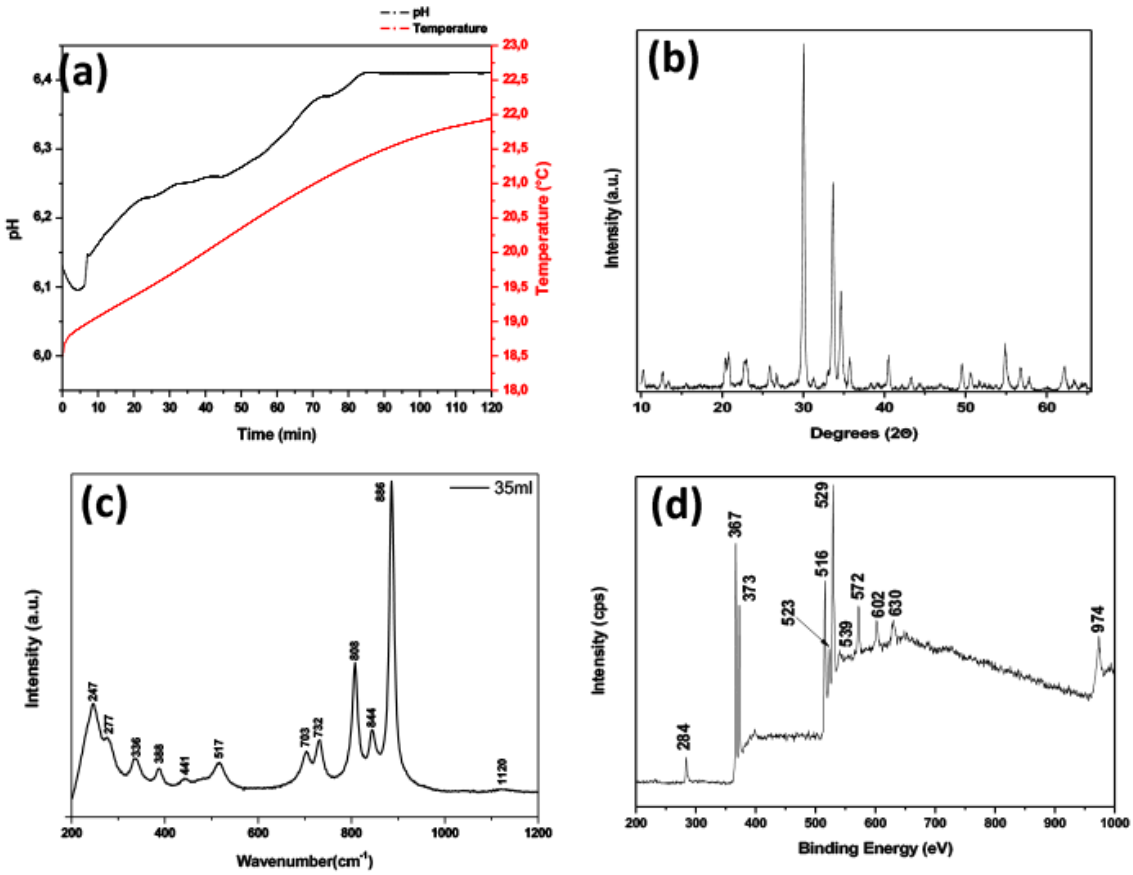

Figure 4: (a) Reaction pH and Temperature vs Time curves during the mixing of the reactants; **(b)** XRD pattern of the as obtained product after hydrothermal treatment; **(c)** Raman; and **(d)** XPS spectra of the as synthesized material.

All the vibrational modes and hence the corresponding Raman peaks are exact match of the pure β-$AgVO_3$ phase as theoretically predicted by Benmokhtar et al [60] and reported by Q. Bao et al. [61, 62]. The recorded vibrational Raman spectra is shown in Figure 4c. In the recorded spectra corresponding Raman peaks of V-O bending modes, symmetric/asymmetric stretching modes of V-O-V bonds and short terminal V=O bonds lie in the range of 300–400 cm^{-1}, ~500 and 700 cm^{-1} and higher than 800 cm^{-1} respectively. The most intense peak at 886 cm^{-1} and a weak band noticed at 844 cm^{-1} are due to the V-O-Ag/ O-V-O vibration and stretching vibrations of VO_3 groups in the $(V_2O_7)^{4-}$ ion respectively. The composition and purity of the as synthesized β-$AgVO_3$ nanowires was examined by XPS measurements as shown in Figure 4d. Various peaks

in the different range of spectrum correspond to the states of carbon, oxygen, silver and Vanadium confirms the formation of β-$AgVO_3$ structure. The peak observed at lower energy value at 284 eV is identified as C 1s bond whereas three peaks situated at 516, 523 and 529 eV correspond to V2p(3/2), V2p(1/2) and O1s respectively. Ag peaks corresponding to the states of Ag3d(5/2) and Ag3d(3/2) are located at 367 and 373 cm^{-1}. All the corresponding peaks of the spectra confirm the formation of β-$AgVO_3$ nanostructure.

Antimicrobial Activity of $AgVO_3$ Nanowires

Figure 5 shows the schematic diagram of the antibacterial activity of the as synthesized materials. The antimicrobial activities of $AgVO_3$ were studied against *Listeria innocua* and *Staphylococcus aureus,* as Gram-positive bacteria, and *Escherichia coli,* as Gram-negative, owing to study the influence of different cellular structure on antimicrobial activity. Antimicrobial results were expressed as log cycles reduction. As Table 1 shows, antimicrobial effect of these nanowires was strongest against *Staphylococcus aureus*, leading to the highest microorganism reduction, followed by bacterial reduction of *Escherichia coli* and *Listeria innocua*. Results were quite interesting because of two main reasons: i) cell reduction occurred at high cell concentrations; working bacterial solutions were modified to 10^8 CFU/ mL, fact that evidenced the enormous antimicrobial activity of these structures; ii) a relation between type of bacteria and antimicrobial activity was not found. Silver nanowires were more active against Gram positive bacteria only in the case of *S. aureus*, because *L. innocua* was found to be less affected than *E. coli* (Gram negative bacteria). Although silver vanadate showed variable efficiency depending the microorganism, antimicrobial capacity of this compound against both bacteria types was hugely stronger than that of common antimicrobial substances, such as natural-based extracts or essential oils. *Thymus* species have been reported to present high inhibition of food-spoilage organisms with values of 900 µg/mL as minimum bactericidal concentration against several microorganisms at 10^5 CFU/ mL, while MBC values of these nanostructures against microorganisms at 10^8 CFU/ mL concentrations were between 50-150 µg/mL [63]. Turnidge et al. [64] studies have also presented minimum inhibition

concentration (MIC) values of excellent antibiotics were between 50-1400 µg/mL, when bacterial working solutions were approximately 1000 times lower.

Regarding to the antimicrobial mechanism of action of these silver vanadate nanostructures, some studies have declared the mechanism of the antimicrobial activity can be derived from the oxidative stress provoked by the production of oxygen reactive species (ROS) such as OH^{*}, $O_2^{\prime}$ and O_2H^{*}. Hydroxyl radicals and protons are formed by water decomposition, and other radicals, such as O_2H^{*} radical, are formed by interaction of protons with oxygen. On the other hand, several vanadate radicals can be also formed, such as $[VO_4]\cdot_d$, $[AgO_4 2Vo^{\cdot}]$, $[AgO_5Vo^{\cdot}]$ and $[AgO_6]^{\prime}$[65]. Other researchers have shown bactericidal action of silver (as Ag^{+} ions or Ag clusters) is due to their strong interaction with thiol groups present in the enzymes involved in bacterial cell metabolism, leading to cell death [66, 67].

Although the exact mechanism of bactericidal action was not yet understood, a proposed mechanism stated that silver nanoparticles in contact with the bacterial cell membrane can be oxidized, and silver ions formed inhibit the action of enzymes responsible for cell metabolism. The presence of silver ions also generates ROS which damage the cells. Due to their acid condition, silver ions present a strong tendency to react with sulfur and phosphorous, compounds present mainly in cell membrane proteins and DNA nucleic acids. This fact attacks cell capacity to replicate. [67, 68] Additionally, the interaction between antimicrobial substances with bacteria is mainly through cell membrane by electrostatic interaction, and several works have associated the effect of changes in antibacterial results with the differences in the morphology of the bacterial membranes [68]. Cell wall of Gram-positive bacteria contains more peptidoglycan, which confers cell rigidity, the outer membrane of Gram-negative bacteria contains lipopolysacharides, which can create a permeability barrier more resistant to antimicrobial compounds but can be also very susceptible to peroxidation. The effectiveness of these antimicrobial structures will be dependent on diffusion and attack of oxidants to the underlying vital sites [69].

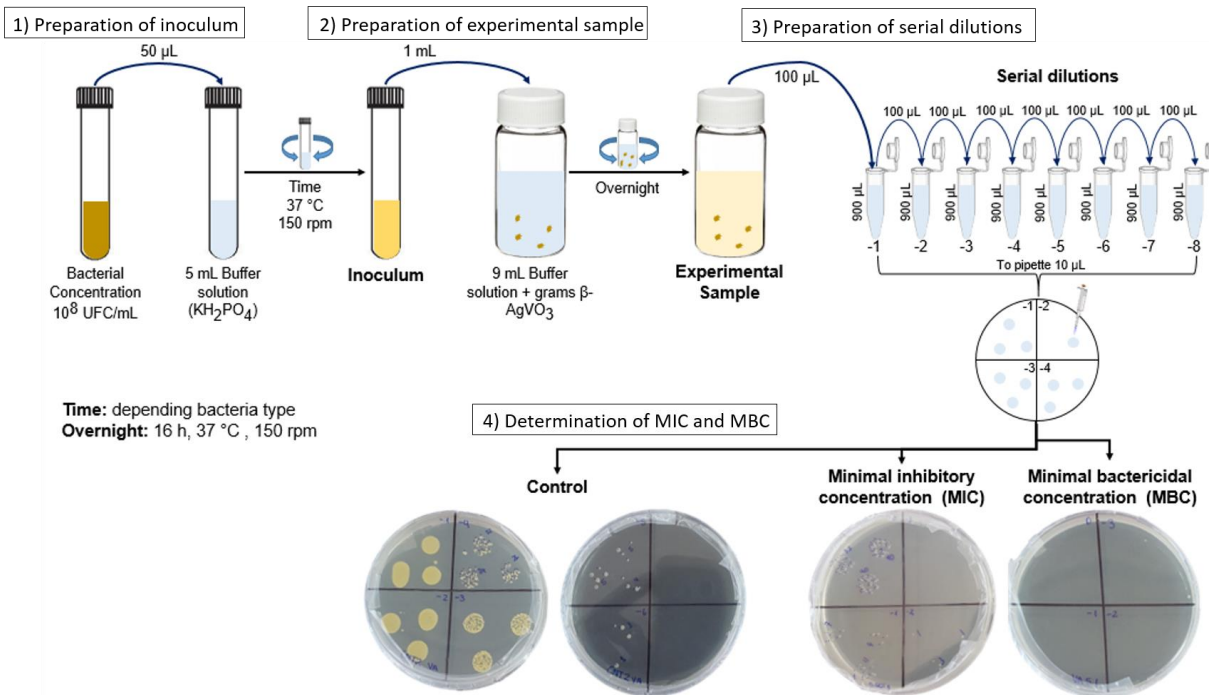

Figure 5. Scheme of methodology used for antimicrobial analysis.

Table 1. Antimicrobial results of as synthesized β-$AgVO_3$ nanowires.

Microorganisms:		*Escherichia coli*		*Listeria innocua*		*Staphylococcus aureus*	
Sample	**$AgVO_3$ (µg/mL)**	**Cel. conc. (UFC/mL)**	**Log reduction**	**Cel. conc. (UFC/mL)**	**Log reduction**	**Cel. conc. (UFC/mL)**	**Log reduction**
Control	0	2.40 E+08	-	2.92 E+08	-	1,43E+08	-
Va 1	25	7.33 E+03	4.6	1.33 E+03	5.3	2,51E+03	4.8
Va2	50	1.63 E+08	5.2	1.80 E+04	4.2	0	8.2
Va3	100	0	8.4	2.87 E+03	5.0	0	8.2
Va4	150	0	8.4	0	8.5	0	8.2

Conclusion

Self-assembly of bulk cylinder interweaved by silver vanadate nanowires is realized by acetonitrile mediated hydrothermal route. The addition of acetonitrile during reaction time not only augmented the surface area of the β-$AgVO_3$ nanostructures up to a remarkable extent but also interestingly shows very high antibacterial activity against Listeria innocua ATCC 33090 and Staphylococcus aureus ATCC 25923 Gram-positive and Escherichia coli ATCC 25922, Gram-negative bacteria. This synthesized material can further be utilized for the study of the various catalytic/photocatalytic and tribological properties to see any enhancement in corresponding behavior. The perfect beaker shaped Macro/nano structure can have future scope of utilization and commercialization as a container for the filtration of bacteria and viruses.

Experimental

Synthesis of Bulk cylinder consolidated ultralong SVO nanorods

All the necessary chemicals and reagents such as ammonium vanadate (NH_4VO_3) silver nitrate ($AgNO_3$) and acetonitrile were of high purity and purchased from Sigma Aldrich. First the 5 mM (~0.0585 g) of NH_4VO_3 solution was prepared in 100 mL of distilled water under constant magnetic stirring to get a homogeneous solution. Separately 10mM (~ 0.1699 g) of $AgNO_3$ solution was prepared into 70 mL of distilled water under stirring to obtain homogeneous transparent solution. Then 30 mL of acetonitrile was added into the 70 ml of $AgNO_3$ solution and stirred for 15 min to obtain a 100 mL solution to maintain 1:1 volumetric ratio with NH_4VO_3. The solution of $AgNO_3$ and acetonitrile was transferred into the NH_4VO_3 solution, under constant magnetic stirring. During the mixing the pH and temperature were also monitored by OAKTON pH and temperature meter until the pH was stable (~ 2 hrs). Optical images were recorded at different time interval of 0, 30, 60, 120 mints to see any visual change in the color of the solution and finally a very light-

yellow color solution was obtained.

Hydrothermal treatment

The obtained very light-yellow color solution after 130 minutes was finally transferred into a 300-mL stainless steel autoclave for hydrothermal treatment. The hydrothermal treatment was done in high temperature box furnace at 150 °C for 10 hrs. After 12 hrs the sample was cooled down to room temperature with a cooling rate of 2 °C per minute which took around an hour more. A yellow color cylindrical structure from bottom to top having cylindrical configuration supported by the wall of the autoclave was observed which was easily transferred into a beaker filled with distilled water. Finally, the obtained bulk cylindrical structure was freeze dried to dry and for further characterizations and application.

Structural/microstructural/spectral characterizations

The as-synthesized materials were characterized by X- ray diffractometer (Shimadzu XRD 6000, 40 kV and 30 mA, Cu-Ka radiation) for structural analysis. Spectral analysis such as Raman and X-ray photoelectron spectroscopies (XPS) were performed to characterize the vibrational modes, as well as chemical bonding. The Raman spectra were recorded using Renishaw inVia Raman microscope with 514 nm laser excitation. The chemical composition was investigated by PHI Quantera XPS, on a PHI-5000C ESCA system with Al Kα X-ray as an excitation source. The shape and morphology of the as-obtained materials were characterized by Zeiss SEM at 30 kV for microstructural characterization without any metal or carbon coating with the fully dried sample loaded on a copper tape.

Antimicrobial activity of $AgVO_3$ nanowires

The antimicrobial activity under dynamic contact conditions of silver vanadate nanowires were tested against *Listeria innocua* ATCC 33090 and *Staphylococcus aureus* ATCC 25923 and *Escherichia coli* ATCC 25922*,* as Gram-positive and Gram-negative bacteria models, respectively, following the International Normative ASTM E2149-10 with some

modifications. Methodology performed is summarized in scheme shown in Figure 5. Bacterial strains were obtained from Biotechnology and Applied Microbiology Laboratory (LAMAP) from the University of Santiago of Chile (Santiago, Chile) and stored in glycerol 30% at -80 °C until needed. For experimental use, the stock cultures were maintained on Tryptone soy agar (TSA) slants at 4 °C and transferred monthly. Prior to each experiment, a loopful of each strain was transferred to 5 mL of Tryptone soy broth (TSB) and incubated at 37 °C for 16 h to obtain fresh early-stationary phase cells. Cell cultures of each microorganism in stationary phase measured at 600 nm were diluted in TSB and incubated at 37 ºC until reach the exponential phase corresponding with a bacterial concentration of 10^8 CFU/ mL. Dilute appropriately into sterile buffer solution to obtain a final concentration of 10^5 CFU/ mL following the normative. Since inhibition was total, the working bacterial solutions was increased to 10^8 CFU/ mL in order to end up with log reduction cycles. $AgVO_3$ solutions were made up in sterile buffer to study the antimicrobial activity expressed as log reduction bacteria, and phosphate buffer solution was used as a control. Compounds were put in contact with bacterial solution and stirred overnight. Then, 10 µL of mixture and serial dilutions of samples in order to quantify microbial population was grown in a Petri dish at 37 °C during 16 h.

Acknowledgements

The author D. P. Singh acknowledge with gratitude the financial support from Millennium Institute for Research in Optics (MIRO), CHILE.

References

1. Masse, R.; Averbuchpouchot, M. T.; Durif, A.; Guitel, J. C. *Acta Crystallographica Section C-Crystal Structure Communications* **1983,** *39*, 1608-1610.
2. Rozier, P.; Galy, J. *Journal of Solid State Chemistry* **1997,** *134*, 294-301.
3. Zhang, S.; Li, W.; Li, C.; Chen, J. *J Phys Chem B* **2006,** *110*, 24855-63.
4. Zandbergen, H. W.; Crespi, A. M.; Skarstad, P. M.; Vente, J. F. *Journal of Solid State Chemistry* **1994,** *110*, 167-175.

5. Kittaka, S.; Matsuno, K.; Akashi, H. *Journal of Solid State Chemistry* **1999,** *142*, 360-367.
6. Lin, H.; Maggard, P. A. *Inorg Chem* **2008,** *47*, 8044-52.
7. Sauvage, F.; Bodenez, V.; Tarascon, J. M.; Poeppelmeier, K. R. *Journal of the American Chemical Society* **2010,** *132*, 6778-6782.
8. Wang, F.; Zhang, H.; Liu, L.; Shin, B.; Shan, F. *Materials Letters* **2016,** *169*, 82-85.
9. Mai, L.; Xu, L.; Gao, Q.; Han, C.; Hu, B.; Pi, Y. *Nano Lett* **2010,** *10*, 2604-8.
10. Lu, J.; Wei, L.; Yao, D.; Yin, X.; Lai, H.; Huang, X. *Journal of the Chinese Chemical Society* **2017,** *64* (7), 795-803.
11. Sang, Y.; Kuai, L.; Chen, C.; Fang, Z.; Geng, B. *ACS Appl Mater Interfaces* **2014,** *6*, 5061-8.
12. Shi, H.; Zhou, C.; Zhang, C. *Research on Chemical Intermediates* **2014,** *41*, 7725-7737.
13. Luster, B.; Stone, D.; Singh, D. P.; to Baben, M.; Schneider, J. M.; Polychronopoulou, K.; Rebholz, C.; Kohli, P.; Aouadi, S. M. *Surface and Coatings Technology* **2011,** *206*, 1932-1935.
14. Mu, Y.; Liu, M.; Wang, Y.; Liu, E. *RSC Adv.* **2016,** *6*, 53043-53053.
15. Singh, D. P.; Polychronopoulou, K.; Rebholz, C.; Aouadi, S. M. *Nanotechnology* **2010,** *21*, 325601.
16. Xin, B.; Yu, Y.; Zhou, J.; Wang, L.; Ren, S.; Li, Z. *Surface and Coatings Technology* **2016,** *307*, 136-145.
17. Zhang, S.; Peng, S.; Liu, S.; Ren, L.; Wang, S.; Fu, J. *Materials Letters* **2013,** *110*, 168-171.
18. Singh, A.; Dutta, D. P.; Ballal, A.; Tyagi, A. K.; Fulekar, M. H. *Materials Research Bulletin* **2014,** *51*, 447-454.
19. Vu, T. A.; Dao, C. D.; Hoang, T. T. T.; Dang, P. T.; Tran, H. T. K.; Nguyen, K. T.; Le, G. H.; Nguyen, T. V.; Lee, G. D. *Materials Letters* **2014,** *123*, 176-180.
20. Liu, S.; Wang, W.; Zhou, L.; Zhang, L. *Journal of Crystal Growth* **2006,** *293*, 404-408.
21. Crespi, A.; Schmidt, C.; Norton, J.; Chen, K. M.; Skarstad, P. *Journal of the Electrochemical Society* **2001,** *148*, A30-A37.
22. Sun, L.; Zhang, Y.; Li, J.; Yi, T.; Yang, X. *Chemistry of Materials* **2016,** *28*, 4815-4820.
23. Singh, D. P.; Yadav, R. M.; Yadav, T. P. *Reviews in Advanced Sciences and Engineering* **2012,** *1*, 319-341.
24. Gao, L.; Li, Z.; Liu, J. *RSC Adv.* **2017,** *7*, 27515-27521.
25. Cao, L. *Materials Letters* **2017,** *188*, 252-256.
26. Abazari, R.; Mahjoub, A. R. *Industrial & Engineering Chemistry Research* **2017,** *56*, 623-634.
27. Zhao, W.; Wei, Z.; He, H.; Xu, J.; Li, J.; Yang, S.; Sun, C. *Applied Catalysis A: General* **2015,** *501*, 74-82.
28. Shi, H.; Zhang, C.; Zhou, C. *RSC Adv.* **2015,** *5*, 50146-50154.
29. Zhang, L.; Yuan, X.; Wang, H.; Chen, X.; Wu, Z.; Liu, Y.; Gu, S.; Jiang, Q.; Zeng, G. *RSC Adv.* **2015,** *5*, 98184-98193.

30. Pan, G.-T.; Lai, M.-H.; Juang, R.-C.; Chung, T.-W.; Yang, T. C. K. *Industrial & Engineering Chemistry Research* **2011,** *50*, 2807-2814.
31. Li, H.; Li, H.; Wu, S.; Liao, C.; Zhou, Z.; Liu, X.; Djurišić, A. B.; Xie, M.; Tang, C.; Shih, K. *Journal of Alloys and Compounds* **2016,** *674*, 56-62.
32. Liang, S.; Zhang, X.; Zhou, J.; Wu, J.; Fang, G.; Tang, Y.; Tan, X. *Materials Letters* **2014,** *116*, 389-392.
33. Liang, L.; Xu, Y.; Lei, Y.; Liu, H. *Nanoscale* **2014,** *6*, 3536-9.
34. Mai, L.; Xu, X.; Han, C.; Luo, Y.; Xu, L.; Wu, Y. A.; Zhao, Y. *Nano Lett* **2011,** *11*, 4992-6.
35. Wei, D.; Li, X.; Zhu, Y.; Liang, J.; Zhang, K.; Qian, Y. *Nanoscale* **2014,** *6*, 5239-44.
36. Du, L.; Zhang, W.; Zhang, W.; Zhang, T.; Lan, H.; Huang, C. *Surface and Coatings Technology* **2016,** *298*, 7-14.
37. Liu, E.; Gao, Y.; Bai, Y.; Yi, G.; Wang, W.; Zeng, Z.; Jia, J. *Materials Characterization* **2014,** *97*, 116-124.
38. Jang, S.-H.; Yoon, J. H.; Huh, Y.-D.; Yoon, S. *J. Mater. Chem. C* **2014,** *2*, 4051-4056.
39. Zhao, Y.; Shao, M.; Que, R.; Zhang, Z. *Journal of Physics and Chemistry of Solids* **2013,** *74*, 255-258.
40. Fu, H.; Yang, X.; Jiang, X.; Yu, A. *Sensors and Actuators B: Chemical* **2014,** *203*, 705-711.
41. Feng, M.; Luo, L.-B.; Nie, B.; Yu, S.-H. *Advanced Functional Materials* **2013,** *23*, 5116-5122.
42. Alivisatos, P. *Nature Biotechnology* **2004,** *22*, 47-52.
43. Patil, M. P.; Kim, G. D. *Applied Microbiology and Biotechnology* **2017,** *101*, 79-92.
44. Zhou, Y.; Kong, Y.; Kundu, S.; Cirillo, J. D.; Liang, H. *Journal of Nanobiotechnology* **2012,** *10*.
45. Le Ouay, B.; Stellacci, F. *Nano Today* **2015,** *10*, 339-354.
46. Franci, G.; Falanga, A.; Galdiero, S.; Palomba, L.; Rai, M.; Morelli, G.; Galdiero, M. *Molecules* **2015,** *20*, 8856-8874.
47. Li, J. L.; Li, Q. H.; Ma, X. Q.; Tian, B.; Li, T.; Yu, J. L.; Dai, S.; Weng, Y. L.; Hua, Y. J. *International Journal of Nanomedicine* **2016,** *11*, 5931-5944.
48. Sadeghi, B. *Journal of Nanostructure in Chemistry* **2015,** *5*, 265-273.
49. Veeraapandian, S.; Sawant, S. N.; Doble, M. *Journal of Biomedical Nanotechnology* **2012,** *8*, 140-148.
50. Wan, W. J.; Yeow, J. T. W. *Journal of Nanoscience and Nanotechnology* **2012,** *12*, 4601-4606.
51. Govindaraju, S.; Ramasamy, M.; Baskaran, R.; Ahn, S. J.; Yun, K. *International Journal of Nanomedicine* **2015,** *10*, 67-78.
52. Hosseini, M.; Mashreghi, M.; Eshghi, H. *Micro & Nano Letters* **2016,** *11*, 484-489.
53. Wang, P.; Zhao, Y. Y.; Tian, Y.; Jiang, X. Y. *Nanomedicine-Nanotechnology Biology and Medicine* **2016,** *12*, 527-528.
54. Jun, S. H.; Cho, S.; Park, Y. *Nanoscience and Nanotechnology Letters* **2015,** *7*, 433-440.
55. Akabayov, S. R.; Akabayov, B. *Inorganica Chimica Acta* **2014,** *420*, 16-23.

56. Chen, T.; Shao, M.; Xu, H.; Wen, C.; Lee, S. T. *J Colloid Interface Sci* **2012,** *366*, 80-7.
57. de Castro, D. T.; Valente, M. L.; da Silva, C. H.; Watanabe, E.; Siqueira, R. L.; Schiavon, M. A.; Alves, O. L.; Dos Reis, A. C. *Arch Oral Biol* **2016,** *67*, 46-53.
58. de Oliveira, R. C.; de Foggi, C. C.; Teixeira, M. M.; da Silva, M. D.; Assis, M.; Francisco, E. M.; Pimentel, B. N.; Pereira, P. F.; Vergani, C. E.; Machado, A. L.; Andres, J.; Gracia, L.; Longo, E. *ACS Appl Mater Interfaces* **2017,** *9*, 11472-11481.
59. Klockner, W.; Yadav, R. M.; Yao, J.; Lei, S.; Aliyan, A.; Wu, J.; Martí, A. A.; Vajtai, R.; Ajayan, P. M.; Denardin, J. C.; Serafini, D.; Melo, F.; Singh, D. P. *Journal of Nanoparticle Research* **2017,** *19*, 288-302.
60. Benmokhtar, S.; El Jazouli, A.; Chaminade, J. P.; Gravereau, P.; Guillen, F.; de Waal, D. *Journal of Solid State Chemistry* **2004,** *177*, 4175-4182.
61. Bao, Q. L.; Bao, S. J.; Li, C. M.; Qi, X.; Pan, C. T.; Zang, J. F.; Wang, W. L.; Tang, D. Y. *Chemistry of Materials* **2007,** *19*, 5965-5972.
62. Bao, S. J.; Bao, Q. L.; Li, C. M.; Chen, T. P.; Sun, C. Q.; Dong, Z. L.; Gan, Y.; Zhang, J. *Small* **2007,** *3*, 1174-7.
63. Cosentino, S.; Tuberoso, C. I. G.; Pisano, B.; Satta, M.; Mascia, V.; Arzedi, E.; Palmas, F. *Letters in Applied Microbiology* **1999,** *29*, 130-135.
64. Turnidge, J.; Kahlmeter, G.; Kronvall, G. *Clinical Microbiology and Infection* **2006,** *12*, 418-425.
65. de Oliveira, R. C.; de Foggi, C. C.; Teixeira, M. M.; da Silva, M. D. P.; Assis, M.; Francisco, E. M.; Pimentel, B.; Pereira, P. F. D.; Vergani, C. E.; Machado, A. L.; Andres, J.; Gracia, L.; Longo, E. *Acs Applied Materials & Interfaces* **2017,** *9*, 11472-11481.
66. Kwakye-Awuah, B.; Williams, C.; Kenward, M. A.; Radecka, I. *Journal of Applied Microbiology* **2008,** *104*, 1516-1524.
67. Holtz, R. D.; Souza Filho, A. G.; Brocchi, M.; Martins, D.; Duran, N.; Alves, O. L. *Nanotechnology* **2010,** *21*, 185102.
68. Morones, J. R.; Elechiguerra, J. L.; Camacho, A.; Holt, K.; Kouri, J. B.; Ramirez, J. T.; Yacaman, M. J. *Nanotechnology* **2005,** *16*, 2346-2353.
69. Dalrymple, O. K.; Stefanakos, E.; Trotz, M. A.; Goswami, D. Y. *Applied Catalysis B-Environmental* **2010,** *98*, 27-38.